OPTICS

Stacking symmetry governed second harmonic generation in graphene trilayers

Yuwei Shan[1], Yingguo Li[1], Di Huang[1], Qingjun Tong[2], Wang Yao[2], Wei-Tao Liu[1,3], Shiwei Wu[1,3]*

Crystal symmetry plays a central role in governing a wide range of fundamental physical phenomena. One example is nonlinear optical second harmonic generation (SHG), which requires inversion symmetry breaking. We report a unique stacking-induced SHG in graphene trilayers, whose individual monolayer sheet is centrosymmetric. Depending on layer stacking sequence, we observe a strong optical SHG in a Bernal ABA–stacked non-centrosymmetric trilayer, while it vanishes in a rhombohedral ABC–stacked one, which preserves inversion symmetry. This highly contrasting SHG due to the distinct stacking symmetry enables us to map out the ABA and ABC crystal domains in an otherwise homogeneous graphene trilayer. The extracted second-order nonlinear susceptibility of the ABA trilayer is surprisingly large, comparable to the best known two-dimensional semiconductors enhanced by excitonic resonance. Our results reveal a novel stacking order–induced nonlinear optical effect, as well as unleash the opportunity for studying intriguing physical phenomena predicted for stacking-dependent ABA and ABC graphene trilayers.

INTRODUCTION

The van der Waals nature of layered crystals can lead to profound effects of stacking order on electronic (*1*, *2*), optical (*3*–*5*), magnetic (*6*), piezoelectric (*7*), and mechanical (*8*, *9*) properties. For instance, the van der Waals stacking evokes a drastic change in nonlinear optical response in atomically thin two-dimensional (2D) materials (*10*–*15*). A notable example is the semiconducting transition metal dichalcogenide MX_2 (M = Mo, W; X = S, Se). Monolayer MX_2 lacks the crystal inversion symmetry and thus permits the electric-dipole allowed second harmonic generation (SHG), which can be further enhanced by excitonic effect (*10*, *11*, *14*, *15*). In sharp contrast, SHG vanishes in Bernal-stacked bilayers or further enhances in rhombohedral-stacked bilayers because of the destructive or constructive interference between neighboring monolayers (*10*, *14*, *15*). Because SHG is highly sensitive to the structural symmetry, SHG spectroscopy and microscopy have emerged as powerful and useful techniques to study these atomically thin materials.

Among the family of 2D materials, graphene is the most prominent material and has the simplest atomic structure. Yet, different from many 2D materials such as hBN, MoS_2, and GaSe (*12*, *13*), graphene monolayers are centrosymmetric with the inversion center at the hollow site of hexagons (Fig. 1A). Thus, no SHG is expected under the electric dipole approximation (*16*). When two centrosymmetric objects are brought together along the same orientation, no matter how they are translated with each other, the composite system remains centrosymmetric. This rule readily applies to the AB-stacked graphene bilayer (Fig. 1B). Therefore, SHG is generally unexpected for graphene bilayers as well, unless the interface and curvature effects or electric-dipole forbidden terms are considered (*16*).

However, crystal symmetry can be readily modified in graphene trilayers. As schematically shown in Fig. 1 (C and D), ABA and ABC graphene trilayers differ on the stacking sequence (*17*, *18*). This difference results in distinct structural symmetries, of which the former is non-centrosymmetric and the latter is centrosymmetric. Therefore, graphene trilayer would provide a platform for exploring a novel nonlinear optical effect, that is, the stacking-induced SHG. While this effect is unique to atomically thin 2D materials, it could be extended to other van der Waals stacked materials with centrosymmetric monolayers such as 1T phase transition metal dichalcogenides (*19*).

Here, we report the observation of emergent electric-dipole allowed SHG in the graphene trilayer with ABA (Bernal) stacking, but it is forbidden in ABC (rhombohedral) stacking. While this difference in stacking order could be captured in their contrasting SHG response, a simple analysis on structural symmetry does not lead naturally to strong SHG. We surprisingly found that the stacking-induced SHG is exceptionally strong, exceeding that of the hBN monolayer (*13*) and even comparable to that of the MoS_2 monolayer upon excitonic resonances (*12*). The ABA trilayer can thus be an outstanding material for exploring nonlinear optical devices. Furthermore, polarization-resolved SHG measurement unambiguously determines the crystalline orientation of ABA trilayers. Because of the distinct stacking symmetry and SHG response between ABA and ABC trilayers, SHG microscopy provides a superior method to image the ABA and ABC domains in graphene trilayers (*20*, *21*). With the aid of this stacking-induced SHG, we believe that many interesting physics predicted for ABA and ABC graphene trilayers could be experimentally explored. These include flat band high-temperature superconductivity (*22*), gate-tunable antiferromagnetic-to-ferromagnetic phase transition (*23*), band topology–associated excitonic physics (*24*), and topologically protected valley-Hall kink and edge states (*25*), and many others (*26*, *27*).

RESULTS

Few-layer graphene samples were prepared by mechanical exfoliation from Kish graphite on a 300-nm SiO_2 on a silicon substrate. Figure 2A shows the bright-field optical microscopy image of a mechanically exfoliated few-layer graphene sample. The layer thickness (monolayer, bilayer, and trilayer) was identified by optical contrast and confirmed by Raman spectra (see fig. S1) (*28*). Upon femtosecond laser irradiation, strong nonlinear optical emission can be detected from graphene. Figure 2B shows the optical emission image of the same area in Fig. 2A, which was excited at 1300 nm with the light emission acquired within 425 to 675 nm. Figure 2C shows the emission spectra from different graphene layers in Fig. 2B. The emission is mainly due to

[1]Department of Physics, State Key Laboratory of Surface Physics, Key Laboratory of Micro and Nano Photonic Structures (Ministry of Education), and Institute for Nanoelectronic Devices and Quantum Computing, Fudan University, Shanghai 200433, China. [2]Department of Physics and Center of Theoretical and Computational Physics, University of Hong Kong, Hong Kong, China. [3]Collaborative Innovation Center of Advanced Microstructures, Nanjing 210093, China.
*Corresponding author. Email: swwu@fudan.edu.cn

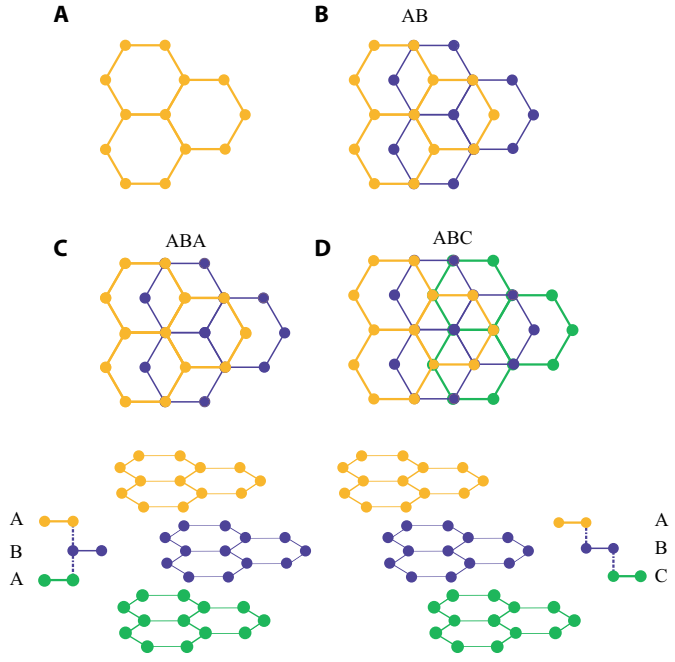

Fig. 1. Stacking orders in few-layer graphene. (**A**) Graphene monolayer. (**B**) AB-stacked graphene bilayer. (**C** and **D**) Two most common polymorphs of a graphene trilayer, ABA (Bernal) and ABC (rhombohedral), respectively. The top, middle, and bottom layers are labeled yellow, purple, and green, respectively. In ABA stacking, the top layer lies exactly on top of the bottom layer; in ABC stacking, one sublattice of the upper layer lies above the center of the hexagons in the lower layer.

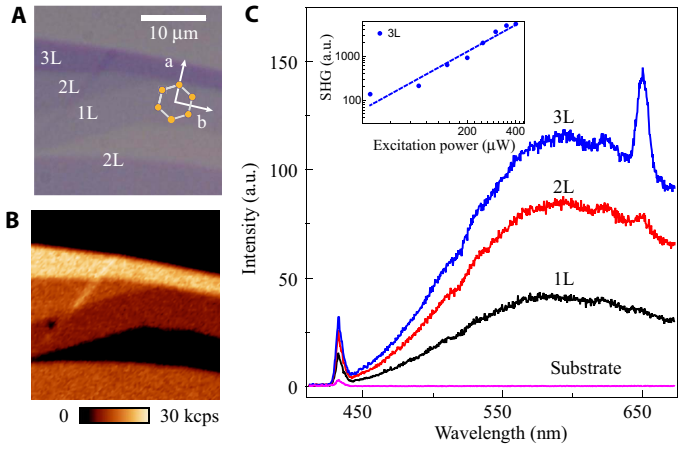

Fig. 2. Optical microscopy and spectroscopy of few-layer graphene. (**A**) Bright-field optical microscopy of mechanically exfoliated few-layer graphene on silicon wafer with 300-nm-thick SiO_2. The crystalline orientation was overlaid on the image, as determined from the azimuthal polarization patterns in Fig. 3. (**B**) Up-converted NPL microscopy of the same area as (A). The sample was excited by femtosecond pulses at a wavelength of 1300 nm and an average power of 0.5 mW without any damages. The collected signal had a spectral range from 425 to 675 nm. (**C**) Corresponding up-converted optical spectra from monolayer (1L), bilayer (2L), trilayer (3L), and bare substrate, respectively. Besides the broad spectra from NPL, THG at 433 nm and SHG at 650 nm were also observed. The inset of (C) plotted the power dependence of SHG, after subtracting the NPL background, on graphene trilayer in a log-log scale. The dotted data were fitted linearly with a slope of 2.02 ± 0.18. a.u., arbitrary units.

an up-converted, broadband nonlinear photoluminescence (NPL) signal, which arises from the Auger-like scattering of photoexcited hot carriers, and its intensity increases proportionally to the layer thickness (*29*, *30*). Besides the NPL, a sharp peak at 433 nm due to the third harmonic generation (THG) was also observed (*31*). As expected, THG is electric dipole–allowed for all graphene layers, and its intensity grows with the layer thickness.

In addition to these known nonlinear optical features, a new and strong peak at 650 nm, twice the energy of the incident photon, emerged from the trilayer (Fig. 2C). To confirm it being SHG, we tuned the excitation wavelength and found the signal to be always at the half-wavelength. We also measured the power dependence of the signal by subtracting the broad background due to NPL. As plotted in the inset of Fig. 2C, the signal intensity grew quadratically with the excitation power, confirming that it is the SHG from graphene trilayer. In comparison to the trilayer, SHG is not observed for the graphene monolayer and nearly absent for the bilayer (Fig. 2C), consistent with their structural inversion symmetry. The weak SHG from the bilayer is likely due to the breaking of inversion symmetry by the substrate or residual doping (*2*).

As we mentioned, although the graphene monolayer, bilayer, and bulk graphite are all centrosymmetric, the overall inversion symmetry can be broken in trilayers of particular stacking orders. This is the case for the ABA (Bernal)–stacked trilayer, which is also the most abundant, naturally existing stacking order. Analogous to a MoS_2 monolayer, the ABA graphene trilayer has a threefold (instead of sixfold) rotation axis along the surface normal and three in-plane twofold (C_2) axes along armchair directions, which belongs to the non-centrosymmetric D_{3h} point group (Fig. 1C) (*10*). Therefore, upon normal incidence, when the excitation polarizer and signal analyzer are set parallel, there should be $I_{SHG}^{XX} \propto |\chi_{aaa}^{(2)} \cos 3\phi|^2$, with $\chi_{aaa}^{(2)}$ being the responsible susceptibility tensor element and ϕ being the angle between the armchair direction and excitation polarization (*10*). When the two polarizations are set perpendicular, we then have $I_{SHG}^{XY} \propto |\chi_{aaa}^{(2)} \sin 3\phi|^2$. These sixfold anisotropies of I_{SHG}^{XX} and I_{SHG}^{XY} are clearly seen in Fig. 3 (A and B, respectively). In comparison, the NPL remains isotropic with respect to ϕ, reflecting the incoherent nature of hot carrier scattering (*29*, *30*). Therefore, the polarization analysis of SHG on the graphene trilayer in Fig. 2A reveals the ABA stacking order and the nature of strong SHG as well. The rotational anisotropy also allowed us to determine the crystal orientation of graphene layers, as shown in Fig. 2A.

In mechanically exfoliated trilayers, there is a common rhombohedral stacking fault leading to the ABC stacking order. It often forms interconnected domains with the ABA trilayer and constitutes only about 15% of the total area (*20*). It is thus difficult to identify the stacking order and different domains noninvasively and accurately. The most widely used technique is Raman spectroscopy and microscopy (*28*). To identify the stacking orders between ABC and ABA, subtle changes in the line shape of various Raman modes (*20*, *21*) or frequency shifts of interlayer shear mode at very low wave numbers (*32*–*34*) are used. Nonetheless, Raman spectra are often weak and highly susceptible to defects, disorders, and strains in the sample that can obscure spectral features (*28*). Furthermore, it is time-consuming to microscopically image the ABA and ABC domains by collecting and analyzing the Raman spectra at each pixel.

Because the ABC trilayer is centrosymmetric and has distinct structural symmetry from the ABA trilayer, no SHG response is expected for the ABC trilayer. Thus, SHG microscopy should be a powerful technique to distinguish the stacking orders. Figure 4A shows the bright-field optical microscopy image of an exfoliated graphene sample on the SiO_2/Si substrate containing both bilayer and trilayer. The entire trilayer region has a uniform contrast in reflectivity. However, on the nonlinear optical

image excited at 1266 nm, different contrasts show up within the same trilayer (Fig. 4B). The contrast of the trilayer region could become uniform again, if we tune the excitation wavelength to 1300 nm so that the SHG signal is no longer in the spectral window (fig. S2). Figure 4C displays emission spectra from the brighter and dimmer regions, respectively. On top of NPL, a prominent SHG peak at 633 nm appears for the brighter region but is absent for the dimmer one, showing the latter to have a centrosymmetric stacking order. The NPL of the brighter region is slightly weaker in the presence of a strong SHG, possibly due to the conservation of oscillator strength. Meanwhile, the SHG rotational anisotropic spectra in Fig. 4 (C and D) prove that the brighter region has a threefold symmetry corresponding to the ABA stacking order and allow us to further determine the crystalline orientation as overlaid in Fig. 4A. To confirm the dimmer and centrosymmetric region to be ABC-stacked, we took Raman spectra, as shown in Fig. 4 (E and F).

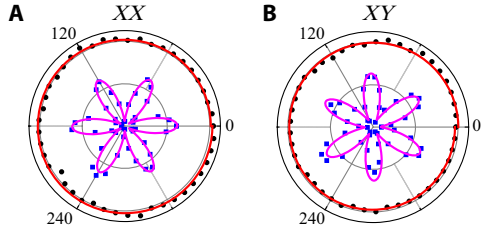

Fig. 3. Azimuthal polarization patterns of SHG and up-converted NPL on the ABA trilayer. (**A** and **B**) The polarizations of the excitation and signal beams are set in parallel (*XX*) and perpendicular (*XY*), respectively. The NPL and SHG signals were shown in black and blue symbols, respectively. The intensity of NPL was integrated from 640 to 660 nm and reduced by 10 times for clarity. While the NPL was fitted with a constant azimuthally, the SHG signals were fitted to functions of $A\cos^2(3\theta)$ and $A\sin^2(3\theta)$ for (A) and (B), respectively.

Compared to the ABA trilayer, the dimmer region has a slightly weaker 2D band, with the spectral weight shifting slightly to lower frequency, consistent with that reported for ABC trilayers (*20*, *21*). Nonetheless, without prior knowledge, it is very difficult to identify the minority ABC stacking based on the subtle differences of the line shape in Raman spectra. SHG clearly yields a much better contrast between the two polymorphs with a high throughput.

Since the inversion symmetry breaking of ABA trilayers is due to the layer stacking, one might consider it as a secondary effect and assume the SHG to be weak. However, by estimating the second-order nonlinear susceptibility described by Zhou *et al.* (*12*), we surprisingly found $|\chi^{(2)}_{aaa}| \sim 0.9 \times 10^{-10}$ m/V (excited at 1300 nm), which exceeds that of the hBN monolayer ($|\chi^{(2)}_{aaa}| \sim 0.3 \times 10^{-10}$ m/V at 900 nm) (*13*) and is even comparable to that of the MoS_2 monolayer ($|\chi^{(2)}_{aaa}| \sim 4.3 \times 10^{-10}$ m/V at 1600 nm and 34×10^{-10} m/V at 1336 nm) upon excitonic resonances (*10*, *12*, *13*). In retrospect, this large optical nonlinearity in the ABA trilayer benefits greatly from the nonlinear optical transitions in resonance with its semimetallic band structure (*17*, *18*), as illustrated in fig. S3. In addition, the large second-order nonlinearity is also in accordance with the strong piezoelectric effect previously observed among few-layer graphene samples (*7*), although the distinct symmetry in the ABA trilayer was overlooked. If the trilayer is ABC-stacked, the strong piezoelectric effect would vanish.

DISCUSSION

The observation of stacking symmetry governed SHG in graphene trilayers permitted the experimental exploration of many intriguing physical phenomena for ABA and ABC trilayers (*17*, *18*, *22*–*27*, *35*). As shown in fig. S4 by following the low-energy effective models (*36*, *37*), the calculated band structures on ABA and ABC graphene trilayers have distinct features. The ABA trilayer is a semimetal with

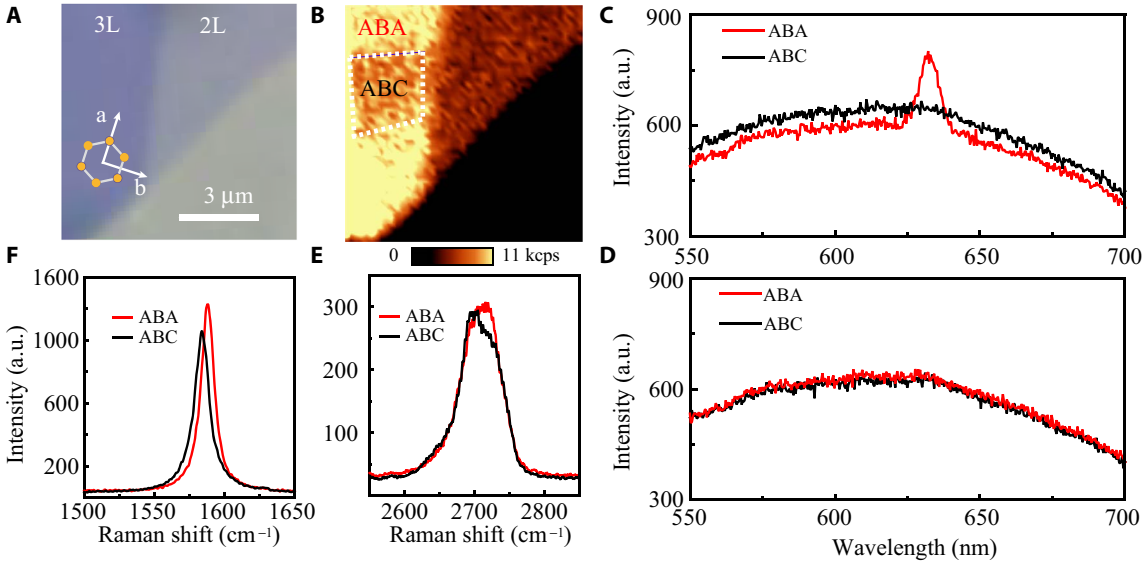

Fig. 4. Imaging the stacking order of ABA and ABC trilayers. (**A**) Bright-field optical microscopy image of few-layer graphene with trilayer on the left and bilayer on the right. The crystalline orientation was also overlaid on the image. (**B**) Corresponding nonlinear microscopy of the same area as (A) with an excitation wavelength of 1266 nm. The spectral band-pass range for the nonlinear signal was centered at 633 nm and narrowed to 6 nm, so that SHG could be more pronounced over NPL. The dwell time at each pixel was 25 ms. The dimmer region from graphene trilayer in (B) is enclosed by dotted lines and attributed to ABC stacking. (**C** and **D**) Nonlinear optical spectra from ABA and ABC trilayer regions, marked in (B), when both the excitation and signal beams were linearly polarized along the armchair or zigzag directions, respectively. (**E** and **F**) Corresponding G and 2D Raman peaks from ABA (red) and ABC (black) trilayers, respectively. The spectra were excited at a wavelength of 532 nm and a power of 1 mW.

gate-tunable band overlap. In contrast, the ABC trilayer is a semiconductor with an electrically tunable bandgap, much like that of the AB-stacked bilayer (*2*). While the electric and optical conductivities have been confirmed by transport and infrared spectroscopy measurements (*17*, *18*, *35*), many more features remain to be explored. For the ABA trilayer, the effect of trigonal warping is significantly stronger than those in the graphene monolayer and the ABC trilayer. With the aid of polarization-resolved SHG to determine the crystalline orientation, the anisotropic response and the role of valley pseudospin (*38*) could be studied. For the ABC trilayer, two nearly flat bands across the gate-tunable bandgap are formed, and the very high density of states at the band edges provides an opens an opportunity for investigating many exotic phenomena (*22*–*25*). The SHG microscopy could help fabricate the high-quality ABC trilayer samples even if they are encapsulated inside hBN (*39*) because the SHG vanishes in even layers of hBN due to Bernal stacking and is weak in odd layers.

METHODS

SHG measurement

The nonlinear SHG measurements were conducted with a custom-built sample scanning confocal optical microscope in a back-scattered geometry. The fundamental beam (120 fs, 80 MHz) was linearly polarized and tunable between 680 and 1300 nm, and focused by a microscopic objective (100×; numerical aperture, 0.95) to the diffraction limit onto the sample at normal incidence. The reflected nonlinear optical signal was collected by the same objective. After passing through a dichroic beam splitter and short-pass (or band-pass) filters, the fundamental beam was filtered out and the nonlinear optical signal was detected by either a single-photon counting silicon avalanche photodetector or a fiber-coupled spectrograph equipped with a liquid nitrogen–cooled silicon charge-coupled device. Nonlinear optical microscopic images were obtained by raster scanning the sample on a piezo-actuated 2D nanopositioning stage. The typical dwell time at each pixel was ~25 ms, more than two orders of magnitude shorter than that used in Raman spectroscopic imaging. To measure the azimuthal anisotropy pattern of the nonlinear optical signal, we rotated the polarization of the fundamental beam with respect to the graphene surface normal using an achromatic half-wave Fresnel rhomb inserted between the dichroic beam splitter and the microscopic objective. The polarization state of the signal beam passing through the same rhomb was analyzed by a linear polarizer in front of detectors. All measurements were carried out in atmosphere and at room temperature.

SUPPLEMENTARY MATERIALS

Supplementary material for this article is available at http://advances.sciencemag.org/cgi/content/full/4/6/eaat0074/DC1

fig. S1. Raman spectra of the sample from a monolayer (1L), a bilayer (2L), and a trilayer (3L), along with the background from the bare substrate.

fig. S2. Comparison of nonlinear microscopy at different excitation wavelengths.

fig. S3. Schematic showing the resonant transitions in the SHG process.

fig. S4. Stacking-dependent properties in ABA and ABC trilayers.

REFERENCES AND NOTES

1. A. H. Castro Neto, F. Guinea, N. M. R. Peres, K. S. Novoselov, A. K. Geim, The electronic properties of graphene. *Rev. Mod. Phys.* **81**, 109–162 (2009).
2. Y. Zhang, T.-T. Tang, C. Girit, Z. Hao, M. C. Martin, A. Zettl, M. F. Crommie, Y. R. Shen, F. Wang, Direct observation of a widely tunable bandgap in bilayer graphene. *Nature* **459**, 820–823 (2009).
3. K. F. Mak, C. Lee, J. Hone, J. Shan, T. F. Heinz, Atomically thin MoS_2: A new direct-gap semiconductor. *Phys. Rev. Lett.* **105**, 136805 (2010).
4. A. Splendiani, L. Sun, Y. Zhang, T. Li, J. Kim, C.-Y. Chim, G. Galli, F. Wang, Emerging photoluminescence in monolayer MoS_2. *Nano Lett.* **10**, 1271–1275 (2010).
5. L. Li, J. Kim, C. Jin, G. J. Ye, D. Y. Qiu, F. H. da Jornada, Z. Shi, L. Chen, Z. Zhang, F. Yang, K. Watanabe, T. Taniguchi, W. Ren, S. G. Louie, X. H. Chen, Y. Zhang, F. Wang, Direct observation of the layer-dependent electronic structure in phosphorene. *Nat. Nanotechnol.* **12**, 21–25 (2017).
6. B. Huang, G. Clark, E. Navarro-Moratalla, D. R. Klein, R. Cheng, K. L. Seyler, D. Zhong, E. Schmidgall, M. A. McGuire, D. H. Cobden, W. Yao, D. Xiao, P. Jarillo-Herrero, X. Xu, Layer-dependent ferromagnetism in a van der Waals crystal down to the monolayer limit. *Nature* **546**, 270–273 (2017).
7. K. Xu, K. Wang, W. Zhao, W. Bao, E. Liu, Y. Ren, M. Wang, Y. Fu, J. Zeng, Z. Li, W. Zhou, F. Song, X. Wang, Y. Shi, X. Wan, M. S. Fuhrer, B. Wang, Z. Qiao, F. Miao, D. Xing, The positive piezoconductive effect in graphene. *Nat. Commun.* **6**, 8119 (2015).
8. K. S. Novoselov, D. Jiang, F. Schedin, T. J. Booth, V. V. Khotkevich, S. V. Morozov, A. K. Geim, Two-dimensional atomic crystals. *Proc. Natl. Acad. Sci. U.S.A.* **102**, 10451–10453 (2005).
9. K. S. Novoselov, A. Mishchenko, A. Carvalho, A. H. Castro Neto, 2D materials and van der Waals heterostructures. *Science* **353**, aac9439 (2016).
10. T. Jiang, H. Liu, D. Huang, S. Zhang, Y. Li, X. Gong, Y.-R. Shen, W.-T. Liu, S. Wu, Valley and band structure engineering of folded MoS_2 bilayers. *Nat. Nanotechnol.* **9**, 825–829 (2014).
11. L. Zhang, K. Liu, A. B. Wong, J. Kim, X. Hong, C. Liu, T. Cao, S. G. Louie, F. Wang, P. Yang, Three-dimensional spirals of atomic layered MoS_2. *Nano Lett.* **14**, 6418–6423 (2014).
12. X. Zhou, J. Cheng, Y. Zhou, T. Cao, H. Hong, Z. Liao, S. Wu, H. Peng, K. Liu, D. Yu, Strong second-harmonic generation in atomic layered GaSe. *J. Am. Chem. Soc.* **137**, 7994–7997 (2015).
13. Y. Li, Y. Rao, K. F. Mak, Y. You, S. Wang, C. R. Dean, T. F. Heinz, Probing symmetry properties of few-layer MoS_2 and h-BN by optical second-harmonic generation. *Nano Lett.* **13**, 3329–3333 (2013).
14. H. Zeng, G.-B. Liu, J. Dai, Y. Yan, B. Zhu, R. He, L. Xie, S. Xu, X. Chen, W. Yao, X. Cui, Optical signature of symmetry variations and spin-valley coupling in atomically thin tungsten dichalcogenides. *Sci. Rep.* **3**, 1608 (2013).
15. N. Kumar, S. Najmaei, Q. Cui, F. Ceballos, P. M. Ajayan, J. Lou, H. Zhao, Second harmonic microscopy of monolayer MoS_2. *Phys. Rev. B* **87**, 161403 (2013).
16. J. J. Dean, H. M. van Driel, Second harmonic generation from graphene and graphitic films. *Appl. Phys. Lett.* **95**, 261910 (2009).
17. C. H. Lui, Z. Li, K. F. Mak, E. Cappelluti, T. F. Heinz, Observation of an electrically tunable band gap in trilayer graphene. *Nat. Phys.* **7**, 944–947 (2011).
18. W. Bao, L. Jing, J. Velasco Jr., Y. Lee, G. Liu, D. Tran, B. Standley, M. Aykol, S. B. Cronin, D. Smirnov, M. Koshino, E. McCann, M. Bockrath, C. N. Lau, Stacking-dependent band gap and quantum transport in trilayer graphene. *Nat. Phys.* **7**, 948–952 (2011).
19. M. Chhowalla, H. S. Shin, G. Eda, L.-J. Li, K. P. Loh, H. Zhang, The chemistry of two-dimensional layered transition metal dichalcogenide nanosheets. *Nat. Chem.* **5**, 263–275 (2013).
20. C. H. Lui, Z. Li, Z. Chen, P. V. Klimov, L. E. Brus, T. F. Heinz, Imaging stacking order in few-layer graphene. *Nano Lett.* **11**, 164–169 (2011).
21. C. Cong, T. Yu, K. Sato, J. Shang, R. Saito, G. F. Dresselhaus, M. S. Dresselhaus, Raman characterization of ABA- and ABC-stacked trilayer graphene. *ACS Nano* **5**, 8760–8768 (2011).
22. N. B. Kopnin, M. Ijäs, A. Harju, T. T. Heikkilä, High-temperature surface superconductivity in rhombohedral graphite. *Phys. Rev. B* **87**, 140503 (2013).
23. B. Datta, S. Dey, A. Samanta, H. Agarwal, A. Borah, K. Watanabe, T. Taniguchi, R. Sensarma, M. M. Deshmukh, Strong electronic interaction and multiple quantum Hall ferromagnetic phases in trilayer graphene. *Nat. Commun.* **8**, 14518 (2017).
24. T. Cao, M. Wu, S. G. Louie, Unifying optical selection rules for excitons in two dimensions: Band topology and winding numbers. *Phys. Rev. Lett.* **120**, 087402 (2018).
25. J. Jung, F. Zhang, Z. Qiao, A. H. MacDonald, Valley-hall kink and edge states in multilayer graphene. *Phys. Rev. B* **84**, 075418 (2011).
26. F. Guinea, A. H. Castro Neto, N. M. R. Peres, Electronic states and Landau levels in graphene stacks. *Phys. Rev. B* **73**, 245426 (2006).
27. S. Yuan, R. Roldán, M. I. Katsnelson, Landau level spectrum of ABA- and ABC-stacked trilayer graphene. *Phys. Rev. B* **84**, 125455 (2011).
28. L. M. Malard, M. A. Pimenta, G. Dresselhaus, M. S. Dresselhaus, Raman spectroscopy in graphene. *Phys. Rep.* **473**, 51–87 (2009).
29. W.-T. Liu, S. W. Wu, P. J. Schuck, M. Salmeron, Y. R. Shen, F. Wang, Nonlinear broadband photoluminescence of graphene induced by femtosecond laser irradiation. *Phys. Rev. B* **82**, 081408 (2010).
30. C. H. Lui, K. F. Mak, J. Shan, T. F. Heinz, Ultrafast photoluminescence from graphene. *Phys. Rev. Lett.* **105**, 127404 (2010).
31. N. Kumar, J. Kumar, C. Gerstenkorn, R. Wang, H.-Y. Chiu, A. L. Smirl, H. Zhao, Third harmonic generation in graphene and few-layer graphite films. *Phys. Rev. B* **87**, 121406 (2013).

32. C. H. Lui, Z. Ye, C. Keiser, E. B. Barros, R. He, Stacking-dependent shear modes in trilayer graphene. *Appl. Phys. Lett.* **106**, 041904 (2015).
33. X. Luo, X. Lu, C. Cong, T. Yu, Q. Xiong, S. Y. Quek, Stacking sequence determines Raman intensities of observed interlayer shear modes in 2D layered materials—A general bond polarizability model. *Sci. Rep.* **5**, 14565 (2015).
34. X. Zhang, W.-P. Han, X.-F. Qiao, Q.-H. Tan, Y.-F. Wang, J. Zhang, P.-H. Tan, Raman characterization of AB- and ABC-stacked few-layer graphene by interlayer shear modes. *Carbon* **99**, 118–122 (2016).
35. M. F. Craciun, S. Russo, M. Yamamoto, J. B. Oostinga, A. F. Morpurgo, S. Tarucha, Trilayer graphene is a semimetal with a gate-tunable band overlap. *Nat. Nanotechnol.* **4**, 383–388 (2009).
36. M. Koshino, E. McCann, Gate-induced interlayer asymmetry in ABA-stacked trilayer graphene. *Phys. Rev. B* **79**, 125443 (2009).
37. F. Zhang, B. Sahu, H. Min, A. H. MacDonald, Band structure of ABC-stacked graphene trilayers. *Phys. Rev. B* **82**, 035409 (2010).
38. D. Xiao, W. Yao, Q. Niu, Valley-contrasting physics in graphene: Magnetic moment and topological transport. *Phys. Rev. Lett.* **99**, 236809 (2007).
39. C. R. Dean, A. F. Young, I. Meric, C. Lee, L. Wang, S. Sorgenfrei, K. Watanabe, T. Taniguchi, P. Kim, K. L. Shepard, J. Hone, Boron nitride substrates for high-quality graphene electronics. *Nat. Nanotechnol.* **5**, 722–726 (2010).

Acknowledgments: We acknowledge Y.-R. Shen and W. Bao for discussions. **Funding:** The work at Fudan University was supported by the National Basic Research Program of China (grant nos. 2014CB921601 and 2016YFA0301002), the National Natural Science Foundation of China (grant nos. 91421108, 11622429, and 11374065), and the Science and Technology Commission of Shanghai Municipality (grant no. 16JC1400401). **Author contributions:** S.W. conceived, designed, and supervised the research project. Y.S., Y.L., and D.H. performed the experiments. Q.T. and W.Y. performed the theoretical calculation on band structures. Y.S., W.-T.L., and S.W. analyzed the data and wrote the manuscript with input from all other authors. **Competing interests:** The authors declare that they have no competing interests. **Data and materials availability:** All data needed to evaluate the conclusions in the paper are present in the paper and/or the Supplementary Materials. Additional data related to this paper may be requested from the authors.

Submitted 16 January 2018
Accepted 27 April 2018
Published 15 June 2018
10.1126/sciadv.aat0074

Citation: Y. Shan, Y. Li, D. Huang, Q. Tong, W. Yao, W.-T. Liu, S. Wu, Stacking symmetry governed second harmonic generation in graphene trilayers. *Sci. Adv.* **4**, eaat0074 (2018).

Stacking symmetry governed second harmonic generation in graphene trilayers

Yuwei Shan, Yingguo Li, Di Huang, Qingjun Tong, Wang Yao, Wei-Tao Liu and Shiwei Wu

Sci Adv **4** (6), eaat0074.
DOI: 10.1126/sciadv.aat0074